



Article (refereed) – Published version

Amoudry, Laurent; Bell, Paul; Thorne, Peter; Souza, Alejandro. 2013 Toward representing wave-induced sediment suspension over sand ripples in RANS models. *Journal of Geophysical Research: Oceans*, 118 (5). 2378-2392. [10.1002/jgrc.20188](https://doi.org/10.1002/jgrc.20188)

This version available at <http://nora.nerc.ac.uk/501471/>

NERC has developed NORA to enable users to access research outputs wholly or partially funded by NERC. Copyright and other rights for material on this site are retained by the rights owners. Users should read the terms and conditions of use of this material at <http://nora.nerc.ac.uk/policies.html#access>

AGU Publisher statement: An edited version of this paper was published by AGU. Copyright (2013) American Geophysical Union. Further reproduction or electronic distribution is not permitted.

Amoudry, Laurent; Bell, Paul; Thorne, Peter; Souza, Alejandro. 2013 Toward representing wave-induced sediment suspension over sand ripples in RANS models. *Journal of Geophysical Research: Oceans*, 118 (5). 2378-2392. [10.1002/jgrc.20188](https://doi.org/10.1002/jgrc.20188)

To view the published open abstract, go to <http://dx.doi.org/10.1002/jgrc.20188>

Contact NOC NORA team at
publications@noc.soton.ac.uk

Toward representing wave-induced sediment suspension over sand ripples in RANS models

Laurent O. Amoudry,¹ Paul S. Bell,¹ Peter D. Thorne,¹ and Alejandro J. Souza¹

Received 11 December 2012; revised 22 March 2013; accepted 1 April 2013; published 9 May 2013.

[1] Parameterizations of near-bed sediment processes are commonly associated with the poor predictive skill of coastal sediment transport models. We implement a two-dimensional Reynolds-averaged Navier-Stokes model to directly assess these parameterizations by reproducing measurements obtained in large-scale wave flume experiments. A sediment transport model has been coupled to wave hydrodynamics and turbulence, and numerical experiments provide temporal and spatial variations of free surface, flow velocity, sediment concentration, and turbulence quantities. Model-data comparisons enable the direct assessment of how key suspension processes are represented and of the inherent variability of the sediment transport model. We focus on the different processes occurring above rippled beds versus dynamically flat beds. Numerical results show that increasing roughness alone is not sufficient to have good predictive capability above steep ripples. Some parameterization of the vortex entrainment process is necessary and a simple modification, which leads to constant sediment diffusivity above steep-rippled beds, is sufficient to obtain good predictions of wave-averaged suspended concentrations. Model-data comparisons for the turbulent kinetic energy are also presented and highlight the need to account for the effect of vortex entrainment on near-bed turbulence and transfer of momentum.

Citation: Amoudry, L. O., P. S. Bell, P. D. Thorne, and A. J. Souza (2013), Toward representing wave-induced sediment suspension over sand ripples in RANS models, *J. Geophys. Res. Oceans*, 118, 2378–2392, doi:10.1002/jgrc.20188.

1. Introduction

[2] Because of limitations in computing resources, numerical models applied to coastal environments generally cannot resolve every process at all scales. This is especially important for coastal sediment transport, for which small-scale near-bed processes are predominant, yet cannot usually be resolved and instead need to be parameterized in some way. This parameterization step is routinely ascribed to the poor predictive capability of models and requires further improvements.

[3] Sea bed ripples are common in sandy coastal and continental shelf environments. These small-scale bed forms are usually generated by waves or a combination of waves and currents and can significantly impact the ambient flow and sediment transport processes. They induce form drag and, therefore, increase the resistance of the bed on the flow. They also can, if steep enough, lead to flow separation

and the formation of vortices, which provides an important mechanism for the suspension of sediment. Following this so-called vortex entrainment process, sediment is trapped in a vortex generated on the lee side of the ripple crest near maximum wave flow velocity. At flow reversal, the vortex is ejected and entrains sediment in suspension [e.g., Thorne *et al.*, 2003]. An important characteristic of this process, compared to sediment entrainment above flat beds, is the coherent nature of the vortex formation and ejection mechanism, which results in strong sediment suspension twice per wave period near flow reversal.

[4] This vortex entrainment process has been observed in the field [e.g., Osborne and Vincent, 1996], and in reduced-scale [e.g., Fredsøe *et al.*, 1999], and large-scale [e.g., Thorne *et al.*, 2003; Hurther and Thorne, 2011; O'Hara Murray *et al.*, 2011] laboratory wave flumes. Intra-ripple hydrodynamics induced by wave flows over steep ripples have been successfully modeled using several approaches such as discrete vortex methods [e.g., Longuet-Higgins, 1981; Hansen *et al.*, 1994; Malarkey and Davies, 2002], Reynolds-averaged Navier Stokes (RANS) models [e.g., Fredsøe *et al.*, 1999; van der Werf *et al.*, 2008], large eddy simulations [e.g., Chang and Scotti, 2004; Zedler and Street, 2006], and direct numerical simulations (DNS) [e.g., Scandura *et al.*, 2000; Blondeaux *et al.*, 2004]. While the DNS approach provides unparalleled details of the intratripple dynamics, it still remains limited to moderate

¹National Oceanography Centre, Joseph Proudman Building, Liverpool, UK.

Corresponding author: L. O. Amoudry, National Oceanography Centre, Joseph Proudman Building, 6 Brownlow Street, Liverpool, L3 5DA, UK. (laou@noc.ac.uk)

Reynolds numbers and cannot address the highly turbulent flows seen in the environment. Further discussions on the relative merits and comparisons between the other approaches can be found in *Chang and Scotti* [2004] and *van der Werf et al.* [2008] for example. The detailed movement of sediment can also be described by either Lagrangian approaches [e.g., *Hansen et al.*, 1994; *Malarkey and Davies*, 2002] or Eulerian approaches [e.g., *Zedler and Street*, 2006; *van der Werf et al.*, 2008]. Models resolving both free surface wave propagation and intrripple dynamics have recently been reported [e.g., *Dimas and Kolokythas*, 2011; *Huang et al.*, 2011], but still remain limited to scaled down systems.

[5] Even though the process of vortex formation and shedding is relatively well understood, a crucial point in coastal modeling is how well it is represented in models that do not resolve the intrripple dynamics. Independent of the turbulence modeling approach employed, multidimensional coastal models still remain too computationally expensive at such high resolution. For example, *Torres-Freyermuth et al.* [2007] employed a resolution of the order of a few centimeters, which is insufficient to fully resolve subripple length scales. Instead, the effect of these bed forms on flow and sediment dynamics needs to be parameterized in some way as the convective nature of vortex entrainment cannot be resolved. Vortex entrainment is generally considered to result in increased mixing for both sediment and momentum, which corresponds to changes in the eddy viscosity (transfer of momentum) and sediment diffusivity (transfer of sediment). Indeed, recent measurements of sediment suspensions have led to profiles of sediment diffusivity which contain both the diffusive component in a Fickian sense and a convective component due to vortex entrainment [*Thorne et al.*, 2009]. These profiles were found to be significantly different above vortex ripples in comparison with above dynamically flat beds. In particular, these observations concurred with *Sleath* [1991] and *Nielsen* [1992], who proposed height-invariant expressions for the time-averaged eddy viscosity in the near-bed layer above steep ripples.

[6] Some representation of modified near-bed mixing has been introduced in simple one-dimensional (1DV) models by implementing algebraic time-dependent specifications of the eddy viscosity and sediment diffusivity, which are prescribed by a series of height-invariant harmonic components [e.g., *Davies and Villaret*, 1999; *Malarkey and Davies*, 2004; *Davies and Thorne*, 2005]. While this approach leads to good predictive power for both wave-averaged and intra-wave behaviors, it still remains unclear how this may be incorporated within multidimensional coastal models that couple complete RANS turbulence closures to sediment transport. In these models, the eddy viscosity is usually computed from the solutions to two turbulence balance equations and the most common approach to include the effects of ripples is to simply treat them as an additional roughness element and to accordingly modify the bed shear stress calculations [e.g., *Amoudry and Souza*, 2011]. This does, in effect, correspond to increasing turbulence and mixing, but the crucial issue as to whether this is sufficient for the type of models considered remains uncertain.

[7] We investigate modeling approaches and parameterizations implemented for wave-induced sediment transport

above ripples. Our objective is to focus on the crucial parameterization of near-bed processes (i.e., the well-understood vortex entrainment) in coastal models that cannot fully resolve them. As such, we do not aim to resolve the intrripple dynamics; instead, we purposely implement a two-dimensional RANS model used at a resolution insufficient to describe the rippled bed in order to focus on the parameterizations of small-scale physical processes. We focus on the RANS approach because of its common usage in coastal applications, and we choose a model which has been developed to reproduce accurately wave propagation and turbulence transport and has been extensively validated [*Lin and Liu*, 1998a, 1998b; *Torres-Freyermuth et al.*, 2007]. Here, we consider transport of noncohesive sand and apply the model to conditions created in a large-scale wave flume experiment [*Williams et al.*, 2000]. We use detailed model-data comparisons of wave velocities, suspended sediment concentration, and turbulence intensity to assess a number of parameterizations. Starting from the known situation of poor predictions above vortex ripples and reasonable predictions above dynamically flat beds, we aim to assess (1) whether the traditional approach of only modifying bed roughness can be sufficient, and (2) whether implementing a more appropriate sediment diffusivity profile is necessary and/or sufficient to improve predictions of wave-averaged suspended concentration profiles.

[8] We first describe the numerical model employed for hydrodynamics and sand transport, as well as its present implementation for several wave conditions over two different sand beds. We then verify the ability of the model to accurately reproduce the wave flows. Model-data comparisons of the suspended sediment concentration are used to assess the sensitivity of the predictions to model parameterizations and constants. Finally, we present estimates of the turbulence intensity and discuss their implications for RANS turbulence modeling.

2. Model Description

[9] The sediment transport model we employ to numerically reproduce the large flume experiments is based on the two-dimensional numerical model CORNELL BReaking wAves and Structure (COBRAS) [*Lin and Liu*, 1998a, 1998b]. The hydrodynamic model solves the two-dimensional RANS equations. The Reynolds stresses are modeled following a $k - \epsilon$ turbulence closure which can use either an isotropic eddy viscosity or the nonlinear stress-strain relationship of *Shih et al.* [1996]. A classical suspended sediment transport model has also been implemented. The full model thus provides temporal and spatial variations of velocity, sediment concentration, and turbulence quantities. We first summarize the governing equations and boundary conditions in their most general form before describing the numerical solution and the implementation of the model for the present study.

2.1. Governing Equations

[10] We assume the fluid to be incompressible and the mean flow field is governed by the following equations using classical tensor notation

$$\frac{\partial \langle u_i \rangle}{\partial x_i} = 0, \quad (1)$$

$$\frac{\partial \langle u_i \rangle}{\partial t} + \langle u_j \rangle \frac{\partial \langle u_i \rangle}{\partial x_j} = -\frac{1}{\rho} \frac{\partial \langle p \rangle}{\partial x_i} + g_i + \frac{1}{\rho} \frac{\partial \langle \tau_{ij} \rangle}{\partial x_j} - \frac{\partial \langle u_i' u_j' \rangle}{\partial x_j}, \quad (2)$$

where $\langle u_i \rangle$ is the Reynolds-averaged velocity in the i th direction, $\langle p \rangle$ is the Reynolds-averaged pressure, u_i' is the turbulent velocity, ρ is the fluid density, which is taken to be constant, and g_i is the i th component of the gravitational acceleration. $\langle \tau_{ij} \rangle$ is the viscous stress tensor.

[11] The Reynolds stress tensor is modeled following the classical isotropic eddy viscosity hypothesis

$$\rho \langle u_i' u_j' \rangle = \frac{2}{3} \rho k \delta_{ij} - \rho \nu_t \langle S_{ij} \rangle, \quad (3)$$

where δ_{ij} is the Kronecker delta and $\langle S_{ij} \rangle$ is the mean rate of strain tensor. The turbulent eddy viscosity, ν_t , is then obtained following

$$\nu_t = C_\mu \frac{k^2}{\varepsilon}, \quad (4)$$

with $C_\mu = 0.09$. The turbulent kinetic energy k and the turbulence dissipation rate ε are computed by solving respective balance equations

$$\frac{\partial k}{\partial t} + \langle u_j \rangle \frac{\partial k}{\partial x_j} = \mathcal{P} - \varepsilon + \frac{\partial}{\partial x_j} \left[\left(\frac{\nu_t}{\sigma_k} + \nu \right) \frac{\partial k}{\partial x_j} \right], \quad (5)$$

$$\frac{\partial \varepsilon}{\partial t} + \langle u_j \rangle \frac{\partial \varepsilon}{\partial x_j} = C_{1\varepsilon} \frac{\varepsilon}{k} \mathcal{P} - C_{2\varepsilon} \frac{\varepsilon}{k} \varepsilon + \frac{\partial}{\partial x_j} \left[\left(\frac{\nu_t}{\sigma_\varepsilon} + \nu \right) \frac{\partial \varepsilon}{\partial x_j} \right], \quad (6)$$

where ν is the kinematic viscosity, \mathcal{P} is the shear production and in which the model constants take the well-known default values $\sigma_k = 1.0$, $\sigma_\varepsilon = 1.3$, $C_{1\varepsilon} = 1.44$, and $C_{2\varepsilon} = 1.92$.

[12] The suspended sediment concentration, c , is computed from an advection-diffusion-settling equation:

$$\frac{\partial c}{\partial t} + \frac{\partial (u_i - w_s \delta_{i3}) c}{\partial x_i} = \frac{\partial}{\partial x_i} \left(K_s \frac{\partial c}{\partial x_i} \right), \quad (7)$$

where w_s is the sediment settling velocity in the vertical direction (x_3 or z) and which is taken to be constant both in space and time. K_s is the turbulent sediment diffusivity and is discussed in more detail in section 2.3.

2.2. Boundary Conditions

[13] At the free surface, boundary conditions enforce zero stress as well as zero normal gradient for turbulence quantities and the sediment concentration. At the bottom boundary, common practice in many coastal models is to employ the rough wall logarithmic law. The friction velocity is then obtained following

$$u_* = \kappa \left[\log \left(\frac{z_b}{z_0} \right) \right]^{-1} u_b, \quad (8)$$

where $\kappa = 0.41$ is the von Karman constant. u_b is the computed horizontal velocity in the first grid cell above the bed, at an elevation z_b above the rough bed of roughness z_0 , which is taken to be the sum of grain and ripple rough-

nesses. The ripple roughness z_{0r} is calculated from the measured ripple dimensions

$$z_{0r} = \frac{a_r \eta_r^2}{30 \lambda_r}, \quad (9)$$

where a_r is a user-defined constant and η_r and λ_r are the ripple height and ripple length, respectively.

[14] For sediment transport under wave or oscillatory flows, the boundary condition for the turbulence quantities may follow two approaches. Turbulent kinetic energy, turbulence dissipation rate, and eddy viscosity can be explicitly related to the friction velocity obtained by equation (8) [e.g., *Savioli and Justesen*, 1997] following

$$k = \frac{u_*^2}{C_\mu}, \varepsilon = \frac{u_*^3}{\kappa z_b}, \nu_t = \frac{\kappa}{C_\mu} u_* z_b. \quad (10)$$

[15] Alternatively, a less constraining condition can be chosen [e.g., *Hagatun and Eidsvik*, 1986; *Amoudry et al.*, 2005] following which:

$$\frac{\partial k}{\partial z} = 0, \varepsilon = \frac{C_\mu^{3/4} k^{3/2}}{\kappa z_b}, \nu_t = C_\mu \frac{k^2}{\varepsilon} \quad (11)$$

[16] The critical difference between these two approaches is that the second allows nonzero turbulent kinetic energy at flow reversal.

[17] For the sediment balance in equation (7), an erosion flux E is specified at the bottom boundary so that

$$-K_s \frac{\partial c}{\partial z} \Big|_{z=z_0} = E, \quad (12)$$

while the settling flux is estimated following an upwind method. In turn, this erosion flux is estimated as a function of the skin-friction component of the bed shear stress. A number of different methods are available but we choose here to implement a reference concentration approach following which $E = c_{\text{ref}} w_s$ [e.g., *Garcia and Parker*, 1991]. We relate the reference concentration to sediment properties and to a Shields parameter θ_c , the nondimensional bed shear stress, that is enhanced from its grain roughness value θ_g , because shear stress varies between ripple crests and troughs

$$\theta_c = \frac{\theta_g}{(1 - \pi \eta_r / \lambda_r)^2}. \quad (13)$$

θ_g is calculated either explicitly from the friction velocity when equation (10) is employed, or using the near-bed value for k instead of the friction velocity when equation (11) is used [e.g., *Amoudry et al.*, 2005].

[18] A large number of reference concentration formulas can be implemented, and we test three expressions. *Thorne et al.* [2002] proposed an empirical formula based on some of the experimental results we aim to reproduce:

$$c_{\text{ref}} = 0.0022 \theta_c^{2.8}, \quad (14)$$

with the reference elevation being at the ripple crest. We also test the reference concentration formulas of *Zyserman*

and Fredsoe [1994] and van Rijn [2007]. The first sets the reference concentration two grain diameters above the mean bed level and the reference concentration is given by

$$c_{\text{ref}} = \frac{0.331(\theta_c - 0.045)^{1.75}}{1 + \frac{0.331}{0.46}(\theta_c - 0.045)^{1.75}}. \quad (15)$$

[19] For our study, the van Rijn approach uses $z_{\text{ref}} = 0.01$ m and the reference concentration is specified as

$$c_{\text{ref}} = 0.015 \frac{d}{z_{\text{ref}}} \left[d \left(\frac{(\rho_s/\rho - 1)g}{\nu^2} \right)^{1/3} \right]^{-0.3} (\theta_c/\theta_{\text{cr}} - 1)^{3/2}, \quad (16)$$

where θ_{cr} is the critical Shields parameter for incipient motion, g is the gravitational acceleration, and d is the sediment particle diameter, taken here to correspond to the experimental median diameter. It has to be noted that the Zyserman and Fredsoe [1994] formulation has not been developed for sediment transport over ripples.

2.3. Sediment Diffusivity

[20] In the model presented so far, the sediment diffusivity is related to the turbulence eddy viscosity following $K_s = \nu_t/\sigma_c$, where σ_c is the Schmidt number. Values are often taken to be less than unity because centrifugal forces tend to eject particles from turbulent eddies [e.g., van Rijn, 1984]. Even though values may depend on the sediment concentration [e.g., Amoudry et al., 2005], concentrations in the present study remain small enough to be able to neglect their influence on the Schmidt number and we then take σ_c to be constant.

[21] However, this default representation of the sediment diffusivity does not take into account the increased mixing due to the vortex entrainment processes. In addition to inducing additional bed roughness, the presence of ripples can modify the vertical profile of the wave-averaged sediment diffusivity. Thorne et al. [2009] computed effective diffusivity values from measurements of sediment concentration with acoustic backscatter systems and observed different profile shapes depending on the slope of the ripples and the occurrence of vortex entrainment. For steep ripples ($\eta_r/\lambda_r > 0.12$), when vortex entrainment occurs, the sediment diffusivity was found to be nominally constant near the bed.

[22] Based on these experimental results, we aim to parameterize the vortex entrainment process by enforcing a constant sediment diffusivity near the bed. In the absence of such a parameterization, the sediment diffusivity is underestimated, and we thus implement a modification fol-

lowing which K_s is taken to have a user-defined minimum value near the bed $K_{s\text{min}}$, i.e.,

$$K_s = \max(K_{s\text{min}}, \nu_t/\sigma_c). \quad (17)$$

[23] By appropriately choosing large minimum values, this scheme ensures a constant and increased diffusivity close to the bed with minimal changes higher in the water column. A number of height-invariant viscosity expressions have been introduced and lead to near-bed sediment diffusivity of the form

$$K_{s\text{min}} = K_{s0} A_0 \omega k_s, \quad (18)$$

where A_0 is the orbital amplitude, ω is the angular frequency, $k_s = 3z_{0r} = a_r \eta_r^2/\lambda_r$ and with different values for the coefficient K_{s0} . Here, we test the height-invariant sediment diffusivity proposed by Nielsen [1992] and Thorne et al. [2009], respectively, $K_{s0} = 0.004/\sigma_c$ and $K_{s0} = 0.0145/\sigma_c$. The specific values employed for $K_{s\text{min}}$ are summarized in Table 1.

2.4. Numerical Solution

[24] The two-dimensional RANS equations are numerically solved following the two-step projection method [Chorin, 1968]. The free surface location is tracked following the volume of fluid (VOF) method [Hirt and Nichols, 1981]. Time derivatives are discretized using a forward time-differencing method. Pressure and stress gradients are discretized using a central difference method, and the advective terms employ a combination of central difference and upwind methods. Similar algorithms are used to solve the two turbulence balance equations and the governing equation for the sediment concentration.

2.5. Model Implementation

[25] We aim to numerically reproduce wave conditions that were obtained in a large-scale flume experiment [Williams et al., 2000]. The model domain represents the flume in two dimensions (x, z) and covers 250 m in the wave propagation direction and 6 m in the vertical direction. Waves are generated within the numerical domain using the internal wavemaker of Lin and Liu [1999] and sponge layers are employed at both lateral boundaries to minimize wave reflection.

[26] The objective of the present study is not to resolve the rippled bed, and the bottom boundary is taken to be a flat bed for which the effect of the ripples is parameterized, as is usually the case in coastal models. This means that the

Table 1. Summary of Wave Heights, Ripple Dimensions, and Sediment Parameters^a

Case	d (μm)	w_s (m/s)	H (m)	d_0 (m)	η_r (m)	λ_r (m)	k_s (m)	$K_{s0} = 0.004/\sigma_c$	$K_{s0} = 0.0145/\sigma_c$
								$K_{s\text{min}}$ (m^2/s)	$K_{s\text{min}}$ (m^2/s)
F1	162	0.0066	0.848	0.75	0.03	0.68	0.0331	1.2×10^{-4}	4.5×10^{-4}
F2	162	0.0066	1.104	0.97	0.07	0.93	0.1317	6.4×10^{-4}	2.3×10^{-3}
C1	329	0.017	0.850	0.75	0.04	0.37	0.1081	4.1×10^{-4}	1.5×10^{-3}
C2	329	0.017	1.111	0.98	0.05	0.43	0.1453	7.2×10^{-4}	2.6×10^{-3}
C3	329	0.017	1.344	1.18	0.06	0.53	0.1698	1.0×10^{-3}	3.7×10^{-3}

^aRipple and wave characteristics correspond to the values reported in Williams et al. [2004]. The settling velocities correspond to median diameter as measured in suspension [e.g., Thorne et al., 2002, 2009].

resolution is not constrained by the ripple dimensions, but rather only needs to be sufficient to resolve the propagation of the wave. A uniform grid size of $\Delta x = 25$ cm and $\Delta z = 5$ cm is used in the present implementation.

[27] Several wave and sediment conditions are then numerically simulated. For each case, wave height (H), wave period (T), mean water depth (h_0), ripple dimensions (λ_r and η_r), and sediment parameters (d, w_s) are specified following the experimental values (Table 1). All cases are such that $T = 5$ s and $h_0 = 4.5$ m. There are, however, some discrepancies within the reported values for the wave height and the ripple dimensions. In particular, different values have been given for H, η_r , and λ_r in *Williams et al.* [2000], *Thorne et al.* [2002], and *Williams et al.* [2004] due to different analysis techniques. It is of little importance for the wave height as the value specified in the numerical model may differ slightly from the experimental value anyway and is chosen to optimize the simulation of the mean wave velocities. But discrepancies for the ripple dimensions result in some uncertainty in the value of the roughness given by equation (9), which is further compounded by a relative lack of agreement in the value of a_r (equation (9)) in the literature. In turn, the uncertainty in the roughness value may lead to uncertainty in the numerical results, which needs to be assessed. We choose to do so by performing the numerical simulations for different sets of ripple dimensions when possible, and different values of a_r .

[28] In addition to the uncertainty in the roughness value, several other parameters of the sediment transport model may induce variability in the numerical results. We focus

on the near-bed boundary conditions employed for turbulence (i.e., using equation (10) or equation (11)) and on the reference concentration formulation (equations (14)–(16)). We also investigate the influence of the value of the Schmidt number and of the sediment settling velocity.

[29] We define a default model configuration as using: Ripple dimensions from *Williams et al.* [2004] (Table 1), $a_r = 25$, equation (10) for the turbulence boundary condition, equation (16) for the reference concentration, $\sigma_c = 0.5$, and the settling velocity following Table 1. The sensitivity of the model is then tested by varying one parameter or condition independently of all others.

3. Numerical Results

[30] The numerical results are compared with experimental data that was collected in the Deltaflume of Delft Hydraulics (now Deltares), Netherlands [*Williams et al.*, 2000]. Horizontal and vertical velocity components are compared with data from five electromagnetic current meters (ECM) fitted to the side wall at five elevations above the bed. Suspended sediment concentrations are compared to data obtained from a side wall mounted pump sample system and from an acoustic backscatter system (ABS) that was deployed on an instrumented tripod platform.

3.1. Default Model Results

[31] Figures 1 and 2, respectively, present the model-data comparison for the phase-averaged flow velocities at five elevations above the sand bed for cases F1, F2, C1, and

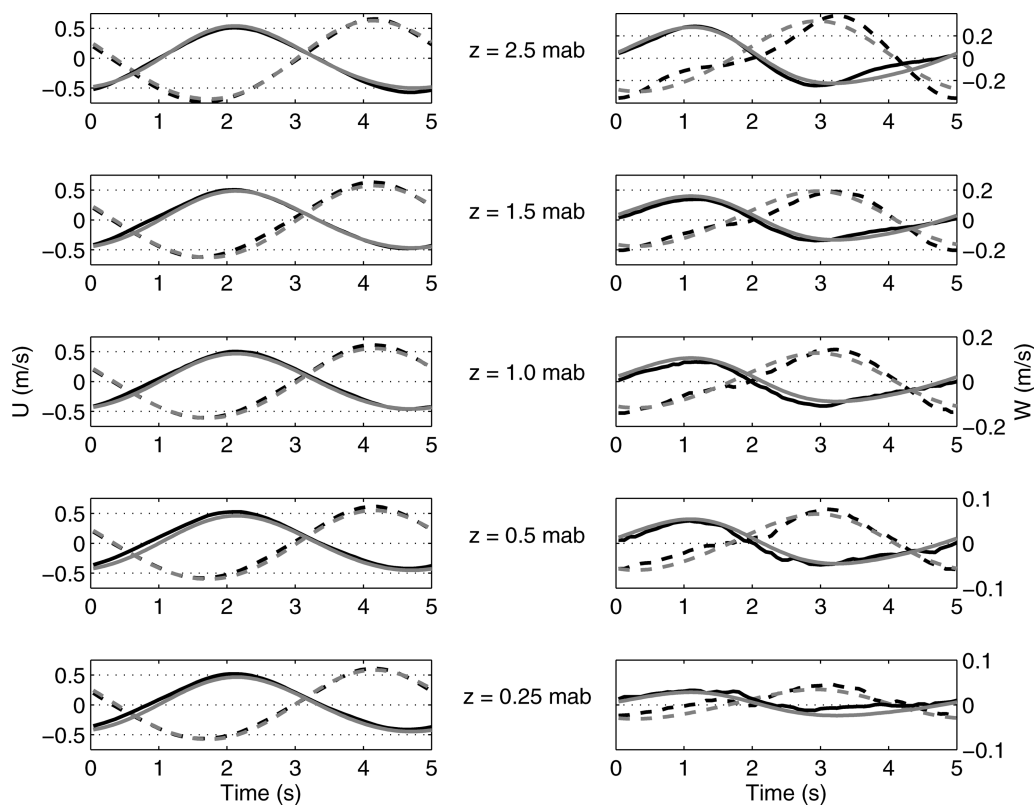


Figure 1. Comparison of modeled (gray line) and measured (black line) values for the (left) horizontal and (right) vertical velocities at five elevations above the bed for case F1 (solid lines) and case F2 (dashed lines).

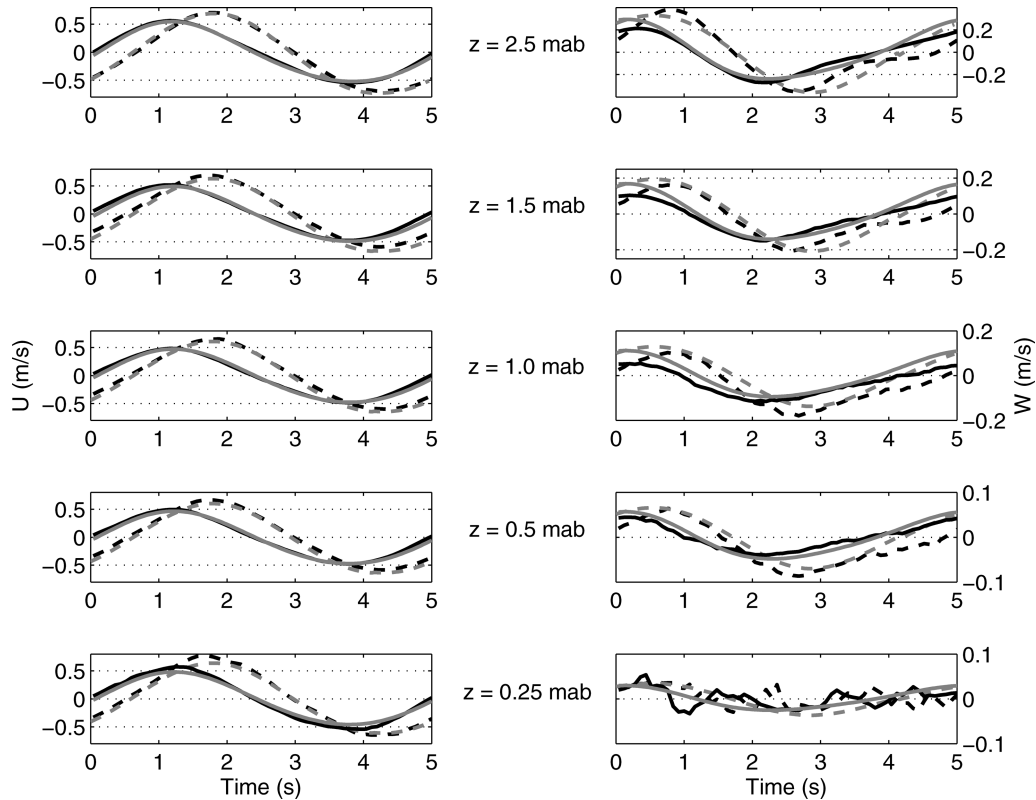


Figure 2. Comparison of modeled (gray line) and measured (black line) values for the (left) horizontal and (right) vertical velocities at five elevations above the bed for case C1 (solid lines) and case C2 (dashed lines).

C2 of Table 1. The phase differences between cases F1 and F2, and C1 and C2 is arbitrary for plotting purposes. The model is in general able to reproduce reasonably well the mean flow velocity. For fine sand, cases F1 and F2 in Figure 1, the comparison is good for both the horizontal and vertical components at all elevations above the bed. For coarse sand, cases C1 and C2 in Figure 2, the comparison is still good for the horizontal component, but worse for the vertical component. In particular, the model does not capture the complexity of the flow at the lowest elevation, which we attribute to not resolving and not parameterizing vortex ejections.

[32] The numerical results for the wave-averaged suspended sediment concentration (SSC) using the default model are shown as the black line in Figure 3 for all cases of Table 1. We find that the model is satisfactory for the fine sand (top row) above the dynamically flat bed, but performs poorly for the coarse sand predictions (bottom row) above steep ripples. Such a behavior may not be unexpected. Could it be that the poor predictions above coarse sand are associated with the default model not resolving nor parameterizing vortex entrainment or by other uncertainties in the model's parameters?

3.2. Model Variability

[33] There may be significant variability in the numerical results due to factors other than that associated with vortex entrainment. It is crucial to estimate variability for both coarse and fine sands in order to properly attribute the effect of the lack of vortex entrainment representation. The

key issue is whether this variability can explain the poor prediction obtained for the coarse sediment. The impact of changing the roughness is presented in Figure 4. Using the ripple dimensions of *Thorne et al.* [2002] results in an increase of about 50% in the roughness value, and the change in the value for a_r corresponds to dividing z_{0r} by about 3. Differences are small overall, limited to the very near-bed region, and changing the roughness does not result in significant improvement of the SSC predictions. This shows that representing the effect of ripples only by increasing the roughness cannot be judged as sufficient if the ripples are steep enough to generate vortex entrainment.

[34] Changing the bottom boundary condition for the flow turbulence is found to impact the sediment concentration profile results as shown in Figure 5. Changing from equation (10) to equation (11) does improve the concentration predictions for the coarse sand but leads to marginally poorer predictions for the fine sand. However, it is not sufficient to entirely justify the poor default results for the coarse sand.

[35] The effect of the reference concentration is summarized in Figure 6. Much like the effect of changing the roughness value, the choice of reference concentration formula is most important in the lower part of the water column, the bottom 20 cm, and does not explain the discrepancy observed for the default setup.

[36] The effect of changing the values of the Schmidt number and the settling velocity are presented in Figure 7. The Schmidt number is halved, and the settling velocities are reduced by about 25%. As expected, reducing either the

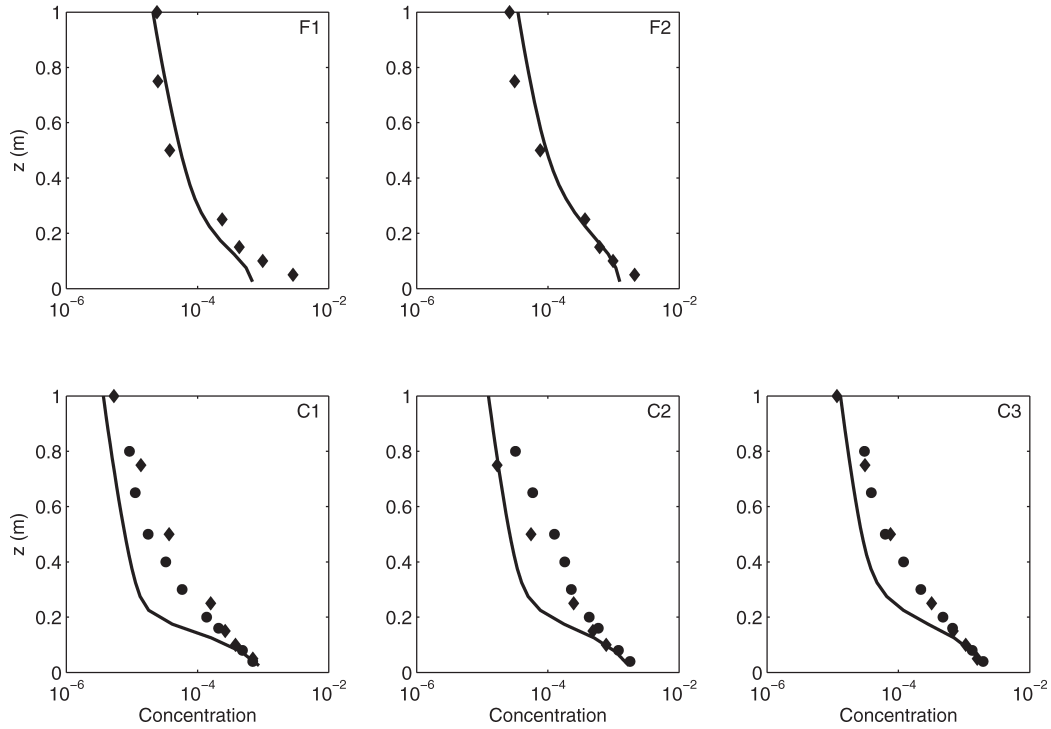


Figure 3. Model-data comparison for the wave-averaged volumetric concentration profiles for all cases of Table 1. Solid circles represent the ABS data from *Thorne et al.* [2002] and the diamonds the pump sample concentrations. The lines are the numerical predictions using the default model setup (see section 2.5).

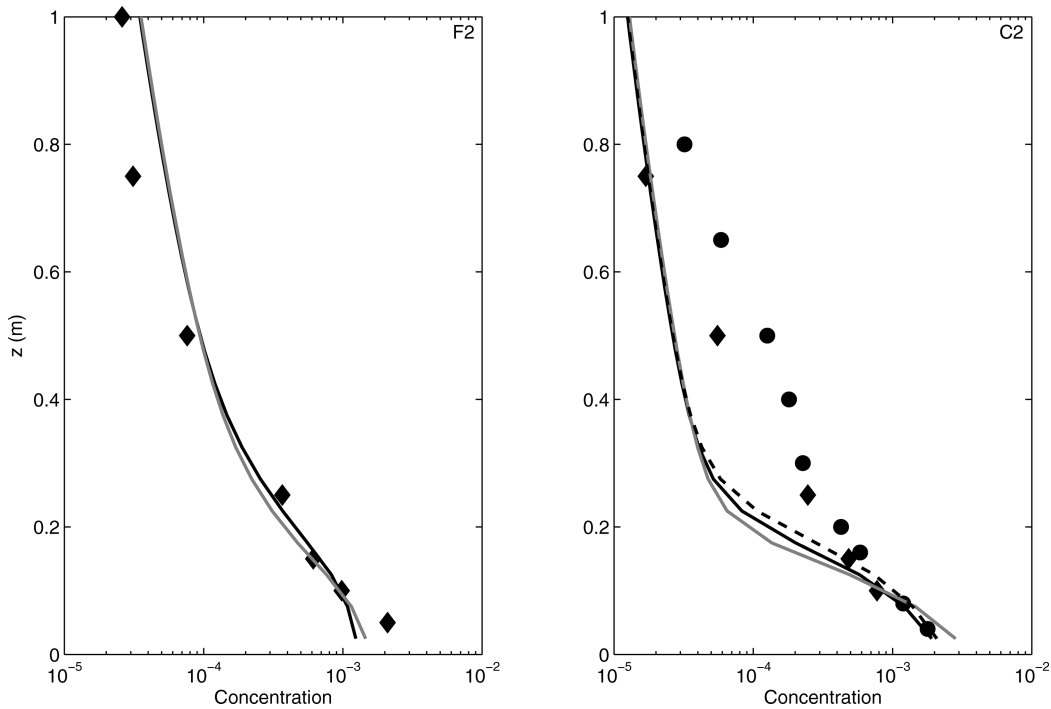


Figure 4. Variability of wave-averaged modeled concentration to changes in roughness for fine sand (case F2, left) and coarse sand (case C2, right). The default simulation is the black line; the dashed line uses the ripple dimensions of *Thorne et al.* [2002], which result in a roughness larger by about 50%; the gray line uses a smaller value $a_r = 8$, i.e., about three times smaller than the default value. Solid circles and diamonds represent experimental data as in Figure 3.

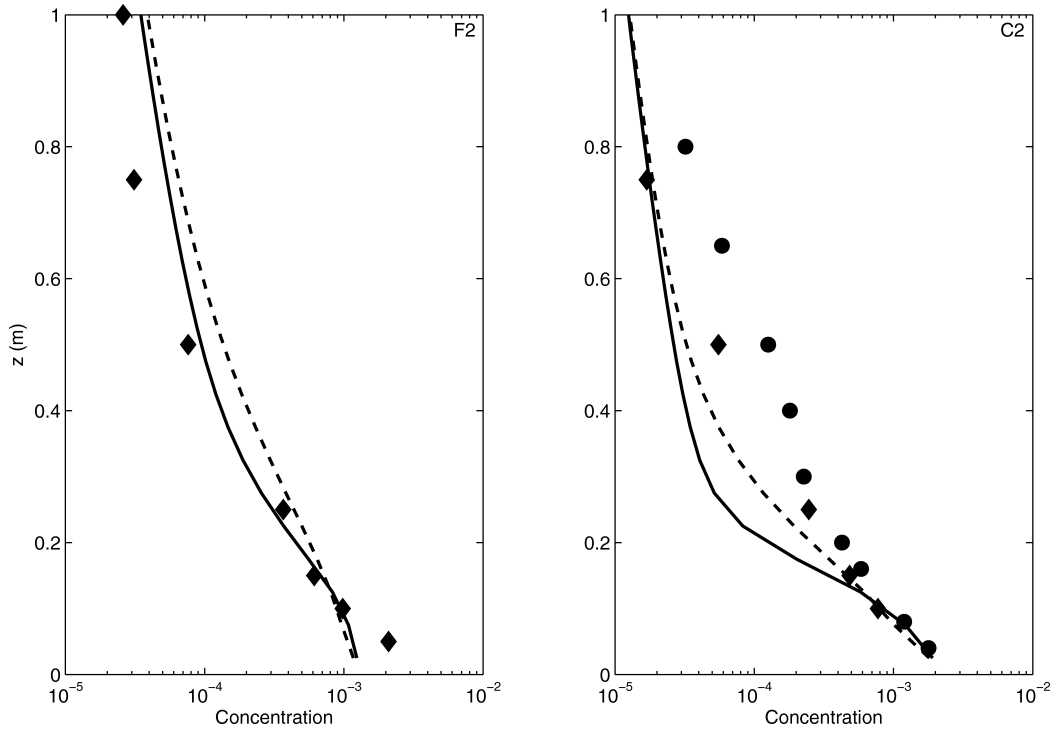


Figure 5. Variability of wave-averaged modeled concentration to turbulence boundary condition for fine sand (case F2, left) and coarse sand (case C2, right). The black line uses equation (10) and the dashed line uses equation (11). Solid circles and diamonds represent experimental data as in Figure 3.

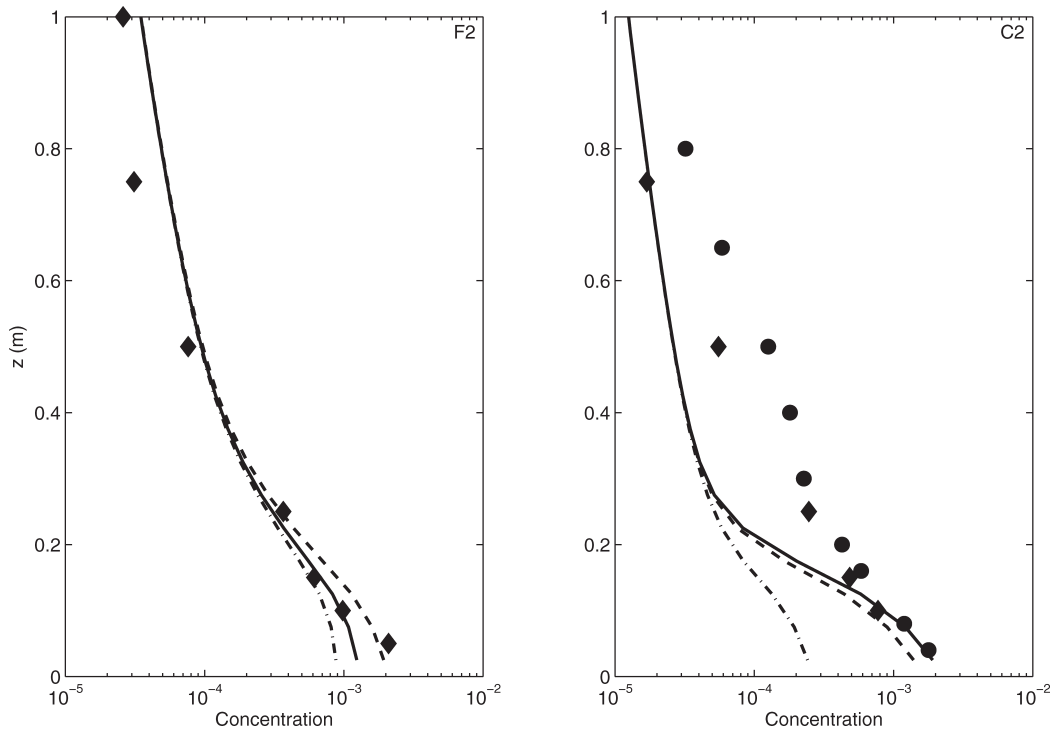


Figure 6. Variability of wave-averaged modeled concentration to formulation of reference concentration for fine sand (case F2, left) and coarse sand (case C2, right). The black line uses the formulation of *van Rijn* [2007], the dashed line the formulation of *Zyserman and Fredsoe* [1994], and the dash-dotted line the formulation of *Thorne et al.* [2002]. Solid circles and diamonds represent experimental data as in Figure 3.

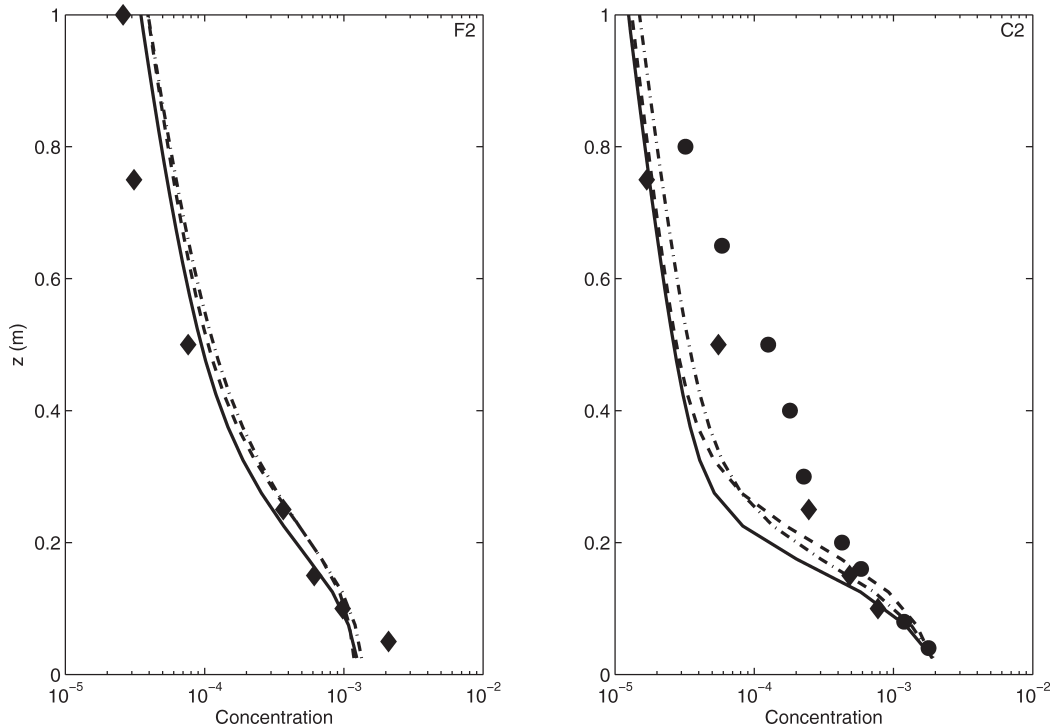


Figure 7. Variability of wave-averaged modeled concentration (volumetric) to changes in suspension parameters for fine sand (case F2, left) and coarse sand (case C2, right). The black line uses the default values for σ_c and w_s ; the dashed line is for $\sigma_c = 0.25$, and the dot-dashed line for a smaller settling velocity ($w_s = 0.013$ m/s for the coarse sand and $w_s = 0.005$ m/s for the fine sand). Solid circles and diamonds represent experimental data as in Figure 3.

Schmidt number value or the settling velocity results in larger suspended sediment concentrations. Smaller values for w_s lead to higher SSC throughout the water column, whereas changing the constant value for σ_c mainly impacts the numerical predictions close to the bed. The global effect is nevertheless not very significant compared with the discrepancies observed between the default numerical results and the experimental values noted in Figure 3.

[37] Overall, numerical predictions of suspended sediment concentrations exhibit sensitivity to all changes considered. Even though the results presented do not consider combinations of changes to several parameters, the sensitivities observed in Figures 4–7 fail to explain the poor results observed for the coarse sand in Figure 3. It also indicates that the fine sand results in Figure 3 can be considered to be within the uncertainty generated by the variability of model parameters.

3.3. Parameterization of Vortex Entrainment

[38] The numerical results for the wave-averaged suspended sediment concentration when using the parameterization of vortex entrainment described in section 2.3 using a constant sediment diffusivity near the bed, as described in equation (18), are presented in Figure 8 alongside the default results. All cases for coarse and fine sands have been simulated for two specific formulations (i.e., *Nielsen* [1992] and *Thorne et al.* [2009]). The proposed modification to the sediment diffusivity profile always leads to significant changes in the predicted wave-averaged sediment concentration profile. For coarse sand, vortex entrainment

is expected to be dominant and the modified model leads to much larger concentrations of suspended sediment. The implementation of the *Thorne et al.* [2009] constant within the default model configuration results in consistent overestimation of suspension, while the using the *Nielsen* [1992] constant lead to good predictions. Conversely, for fine sand, vortex entrainment is not the dominant process and the default model should produce the better predictions. For case F1, the minimum diffusivity determined following *Nielsen* [1992] is small enough not to impact much the overall computations, due to the very low roughness from the ripple dimensions. Case F2 presents a rougher dynamically flat bed and the default model does indeed produce the better results.

[39] The modified model also exhibits variability to model parameters. While we do not present all effects here, the impact of changing the Schmidt number and the settling velocity are presented in Figure 9 for case C1. Similar to the results presented in Figure 7, reducing σ_c and w_s results in higher suspended concentration. Taking into account this variability, the model using the modified sediment eddy diffusivity can be considered to reproduce well the experimental data for the coarse sand.

4. Toward Modeling Near-Bed Turbulence and Sediment Diffusivity

[40] The numerical results presented in the previous section show that predictions of suspended sediment concentration suffer from nonnegligible variability due to

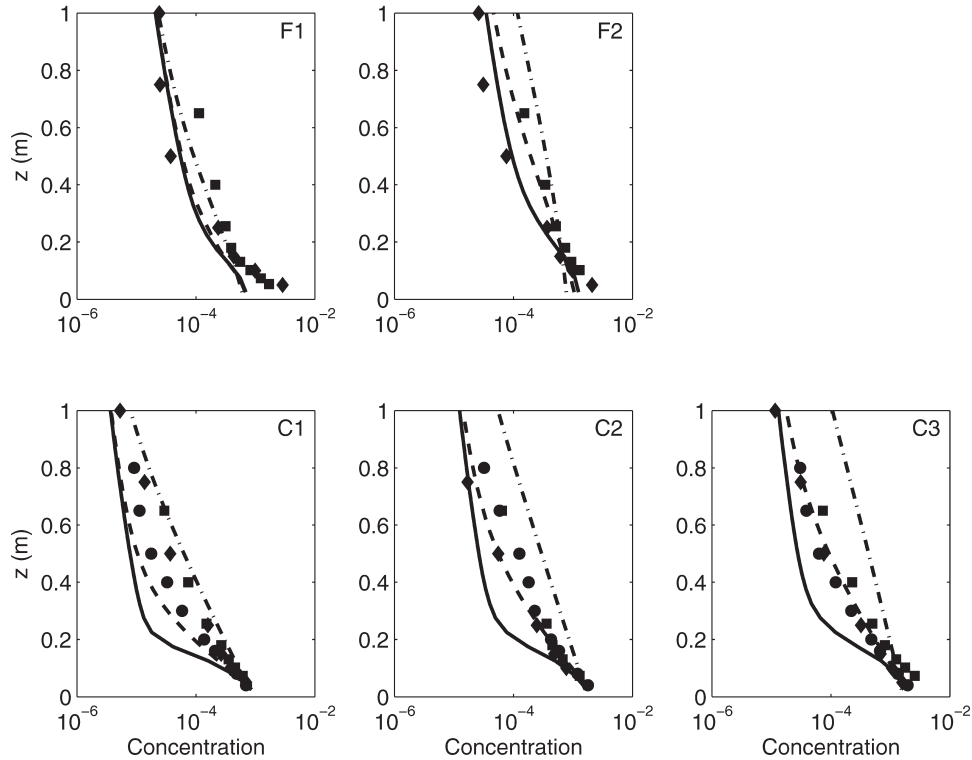


Figure 8. Model-data comparison for the wave-averaged volumetric concentration profiles for all cases of Table 1. Solid circles represent the ABS data from *Thorne et al.* [2002] and the diamonds the pump sample concentrations. The solid lines are the numerical predictions using the default model setup (see section 2.5); the results with implementation of vortex entrainment following equations (17) and (18) are plotted as dashed lines for $K_{s0} = 0.004/\sigma_c$ [Nielsen, 1992], and as dash-dotted lines for $K_{s0} = 0.0145/\sigma_c$ [Thorne et al., 2009].

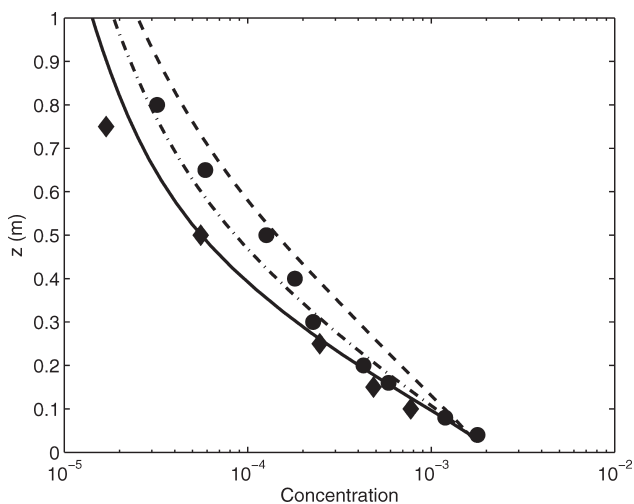


Figure 9. Model variability for wave-averaged concentration, when vortex entrainment is parameterized over coarse sand following equations (17) and (18) with $K_{s0} = 0.004/\sigma_c$ (case C2). The black line uses default values $\sigma_c = 0.5$ and $w_s = 0.017$ m/s; the dashed line results from a change of Schmidt number only to $\sigma_c = 0.25$; and the dot-dashed line results from a smaller settling velocity $w_s = 0.013$ m/s. Solid circles and diamonds represent experimental data as in Figure 3.

uncertainty in some model parameters. This variability is found to be larger than the model-data discrepancy for the fine sand, and the default predictions can thus be considered as satisfactory. This is, however, not the case for the coarse sand, and using a modified sediment diffusivity is necessary to obtain good predictions. An appropriate specification for K_s is crucial to the SSC predictions, and depends on the presence and type of bed forms.

[41] In essence, we attribute the poor SSC predictions to inappropriate description of the sediment diffusivity K_s or, in other words, poor modeling of turbulent suspension. In turn, erroneous sediment diffusivity may be due to incorrect Schmidt number σ_c or poor modeling of the eddy viscosity. Even though the sensitivity to different constant values for σ_c was not able to explain the discrepancies for coarse sand, more advanced Schmidt number formulations do exist. In this section, we present turbulence data with the aim of identifying the main shortcoming in turbulence and turbulent suspension modeling.

4.1. Turbulent Kinetic Energy Model-Data Comparisons

[42] We undertake here model-data comparisons of wave-averaged turbulent kinetic energy (TKE). We estimate experimental values from the velocity data measured with ECMs. Only two components, u and w , are available

and we take the measured TKE, k_e , to be [e.g., *Hurther and Thorne, 2011*]:

$$k_e = \frac{3}{4}(\sigma_u^2 + \sigma_w^2), \quad (19)$$

where σ_u and σ_w are the turbulence intensities in the horizontal (along flume) and vertical directions. The measured velocity data contain both wave and turbulence contributions, and estimating the TKE requires removing the contribution from the waves. We choose here to employ a very simple filtering technique. The data was obtained for regular waves of known frequency. We thus removed the wave contribution by filtering out the fundamental frequency (corresponding to $T = 5$ s) and the first two harmonics since the wave was nonlinear.

[43] The resulting values for the turbulent kinetic energy are presented in Figure 10, along with modeled profiles. For similar wave heights (e.g., cases C1 and F1, cases C2 and F2), the turbulence is experimentally observed to be relatively independent of the bed type except close to the bed, where the measured TKE over the coarse sand vortex ripples is significantly larger than that over the fine sand dynamically flat bed. The measurements in Figure 10 highlight an increase of at least one order of magnitude at a distance of 25 cm above the bed. These results 25 cm above the bed are not only well outside of the traditional wave boundary layer, but also outside the range where vortices may be expected, i.e., one to two ripple heights above the crest [e.g., *Malarkey and Davies, 2004*]. This clearly shows that vortices have an impact on hydrodynamics (both on velocity components as shown in Figure 2 and on wave-averaged turbulence in Figure 10) at elevations significantly higher up in the water column than was previously

thought and has previously been implemented in 1DV models such as that of *Davies and Thorne [2005]*.

[44] Examples of the power spectra of unfiltered velocity components S_{uu} and S_{ww} are given in Figure 11. All spectra are very similar and approximate a simple negative power spectrum at frequencies over 1 Hz. The sole exception is the two spectra at the lowest elevation above the coarse sand vortex ripples, which is an indication of the different mechanisms at play above the two beds and their influence on the hydrodynamics. The presence of higher harmonics of the fundamental wave frequency in S_{ww} is another manifestation of the coherent processes involved. The larger TKE values observed close to the bed in Figure 10 also correspond to the significantly different shape of the spectra at $z = 0.25$ m.

[45] Far from the bed ($z \geq 1$ m), the model produces larger TKE values compared with observations, which could be a consequence of the filtering technique applied to the data removing more than just the wave contribution. Close to the bed, we observe a difference in model-data agreement depending on the bed conditions. Above the dynamically flat bed, the model-data comparisons are quite satisfactory. Above the vortex ripple bed, there is reasonable agreement at $z = 0.5$ m and clear underestimation by the model at $z = 0.25$ m.

4.2. Toward Better Modeling of Mixing Above Ripples

[46] These results strongly suggest that the turbulence model is deficient in some way, which is not entirely surprising given the physical processes at play. In particular, the failure of the model to reproduce the larger turbulence above the vortex ripple bed is critical, as the vortices generated in this case entrain both sediment and momentum, and result in increased mixing for both. While this failure is not

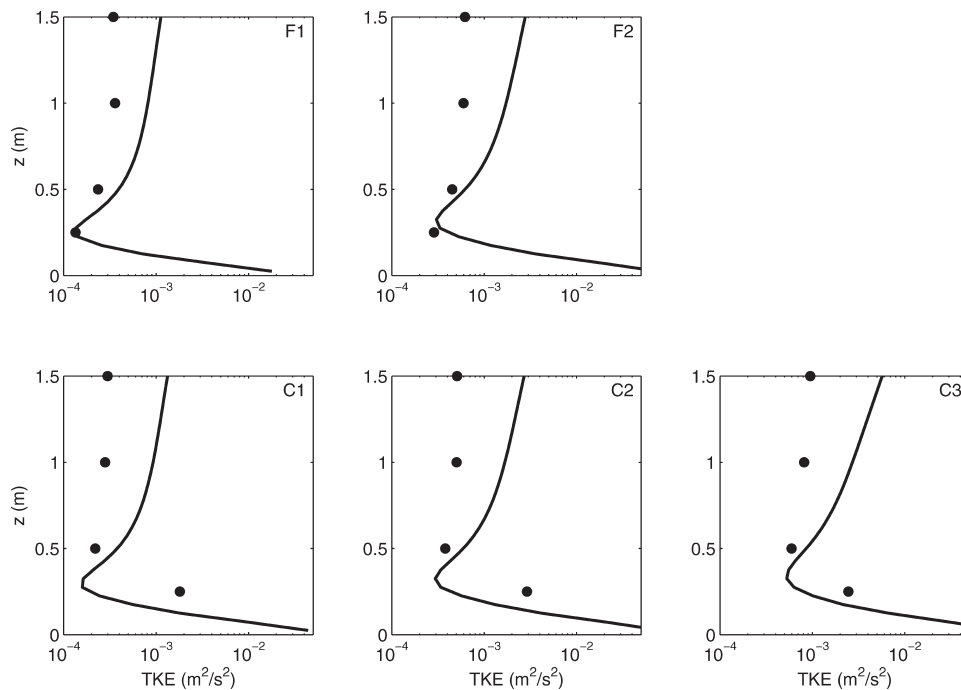


Figure 10. Model (line) data (circles) comparison for the wave-averaged turbulent kinetic energy profiles for all cases of Table 1.

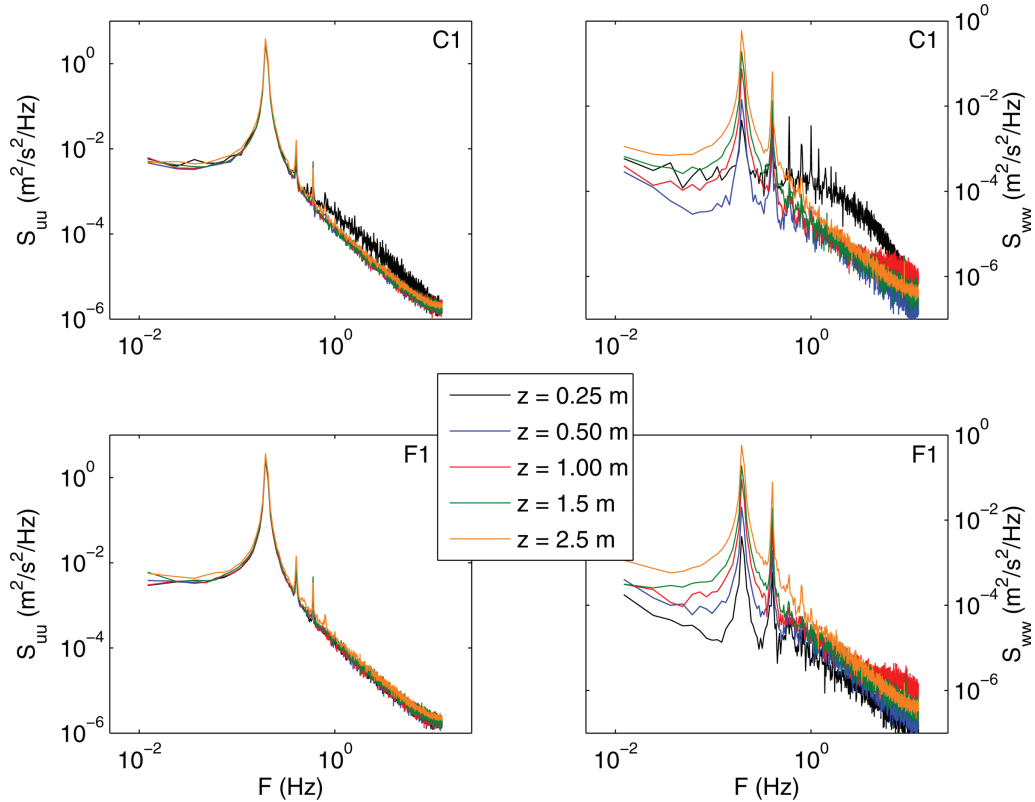


Figure 11. Spectra for the (left) horizontal, S_{uu} , and (right) vertical, S_{ww} , components of the velocity for (top) cases C1, and (bottom) F1. The spectra are from data at five elevations above the bed: $z = 0.25$ m in black; $z = 0.50$ m in blue; $z = 1.00$ m in red; $z = 1.5$ m in green; and $z = 2.5$ m in orange.

unexpected given that vortex formation and ejection are neither resolved nor parameterized, the resulting underestimation of turbulent mixing can be clearly linked to the predicted erroneous steep concentration gradient observed in Figure 3.

[47] The RANS model used here does have known deficiencies and issues. It does not account for buoyancy production due to sediment-induced stratification. This term is negative for sediment suspensions with concentration decreasing with elevation and results in turbulence damping. We also did not include a dependence on the concentration in equation (4), but the concentrations we have considered remain too small for this to have a significant effect. Finally, we used an isotropic model for the eddy viscosity. We have tested this assumption by using the nonlinear stress-strain relationship of *Shih et al.* [1996], but did not find any improvement on either the TKE or the SSC predictions. None of these issues can, therefore, explain the poor results, and introduce the necessary differences above vortex ripples.

[48] Near-bed vortex influenced mixing has been implemented here solely by changing the sediment diffusivity. A similar scheme applied to the eddy viscosity instead of the diffusivity (i.e., applying equation (17) to ν_t instead of K_s) does not result in significant improvement of near-bed SSC predictions (Figure 12). Implementing the minimum value on ν_t , the resulting near-bed viscosity is both height-invariant and constant in time. The wave-averaged TKE profiles are modified, but still do not match the observed increase at

$z = 0.25$ m (Figure 12). This model-data comparison shows that it is clearly insufficient to prescribe constant and height-invariant viscosity above vortex ripples.

[49] This is not incompatible with the previous modeling studies of *Davies and Villaret* [1999] and *Davies and Thorne* [2005], in which a time-dependent viscosity was algebraically prescribed. The present work does not test such time-dependent algebraic formulation for ν_t , as this would be redundant with the turbulence closure scheme under the RANS-VOF framework. Better modeling of mixing above vortex ripples in multidimensional coastal models may result from either future extension of 1DV algebraic eddy viscosity, or modifications to existing turbulence closure schemes. We believe that a detailed discussion on the relative merits of each approach is beyond the scope of the present work, but that it should involve considerations of completeness, cost and ease of use, and range of applicability.

[50] Concerning potential modification to turbulence closure schemes, the different shapes observed for the velocity spectra imply different mechanisms related to the coherent structures above steep ripples. Indeed, the turbulence dynamics above vortex ripples is characterized by coherent energetic ribs, which are generated by stretching of the vortices created by the flow above the steep ripples [*Blondeaux et al.*, 2004]. This process is commonly associated with turbulence production, which is not accounted for in RANS models at the scale employed here. High dissipation is another important feature of turbulence above vortex

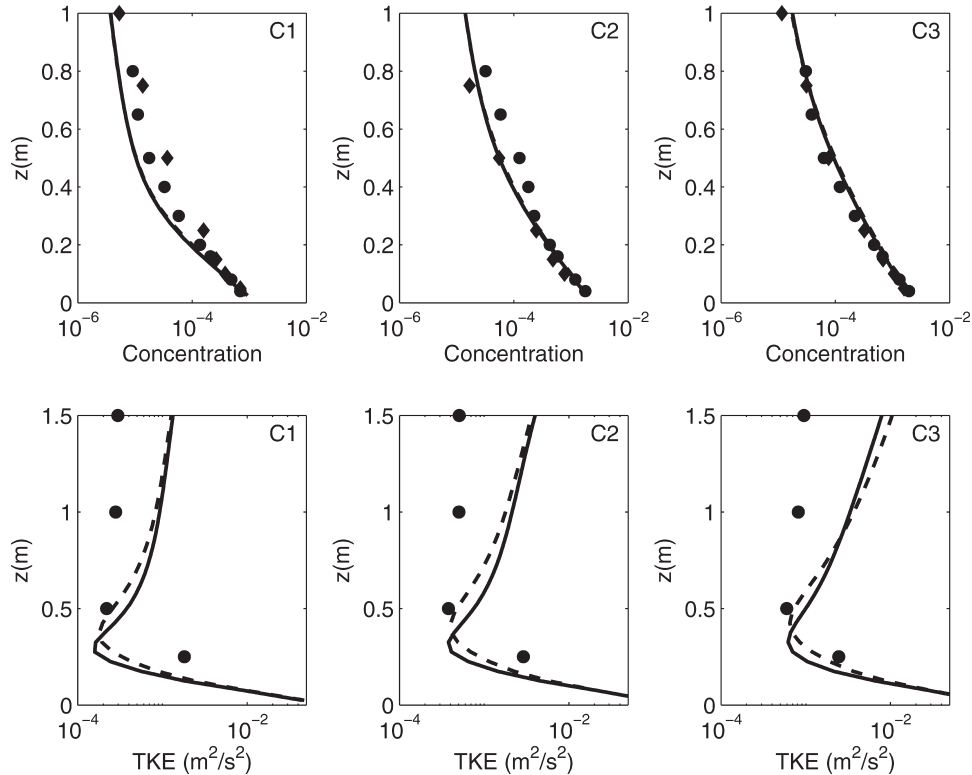


Figure 12. (top row) Model-data comparison for wave-averaged concentration and (bottom row) wave-averaged turbulent kinetic energy above vortex ripples (cases C1, C2, and C3). Solid line: model using minimum eddy diffusivity; dashed line: model using minimum eddy viscosity; and symbols: experimental data. Both model implementations use *Nielsen* [1992] constants.

ripples [e.g., *Barr et al.*, 2004; *Blondeaux et al.*, 2004]. We, therefore, expect these to require modifications to the balance equations employed by RANS schemes at the coastal scale. The model-data comparisons (Figures 10 and 12) show a consistent underprediction of near-bed turbulence, and we would thus expect to require an additional productive term to better match the TKE data. One possible option would, therefore, be to introduce an extraproduction term which would be (1) limited to the near-bed region and (2) a function of the ripples' characteristics. Interestingly, this is somewhat analogous to the approach advocated by *Mellor* [2002] to include the effect of oscillatory flow on mean currents and would also modify the near-bed dissipation.

4.3. Intraday Variations for Sediment Suspension

[51] We have so far focused on wave-averaged suspended sediment. From a practical point of view, this can probably be considered as sufficient if the main interest lies in the effect of suspended sediment in relation to quantities evolving significantly slower than the wave period. However, considering wave-averaged quantities is not sufficient to determine the total sediment transport rate, which also has a wave-related component. In this case, how suspension correlates with the flow velocity is fundamental and intraday analyses are important. Even though we reiterate that the main focus of the present study deals with the ability to predict wave-averaged suspension profiles and the implied modeling requirements, we now briefly discuss intraday variations.

[52] Experimental studies have shown that, above vortex ripples, two suspension maxima occur near flow reversals with a stronger event linked to the onshore to offshore reversal [e.g., *Thorne et al.*, 2003]. It has to be pointed out that our model typically fails to qualitatively reproduce this behavior above the coarse sand bed. This was not found to be improved by any of the changes introduced in this study. Poor intraday parameterizations of sediment pickup and near-bed mixing both impact the overall numerical simulations and may justify poor model performance. When pickup is directly related to the friction velocity, as is most commonly the case including here, near-bed concentration maxima occur near maximum wave flow. This obviously cannot result in the correct intraday suspension patterns above steep ripples when vortex entrainment occurs.

[53] We also tested the approach implemented in *Amoudry et al.* [2005] following which the pickup rate is related to the near-bed turbulence. However, a qualitatively incorrect intraday behavior was again observed. It is unfortunately not possible to determine whether this is due to the sediment pickup boundary condition or to the deficiencies in the turbulence model. However, it has to be pointed out that other intraday formulations of sediment pickup have been considered. *Vittori* [2003] found that sediment pickup rate showed a large hysteresis when related to the friction velocity and suggested that it be related to TKE production instead. *Amoudry and Liu* [2010] linked the net sediment flux at the bed, the sum of erosion and deposition, to accelerating flow. Figure 13 presents typical intraday variations of free stream velocity, friction velocity and near bed TKE

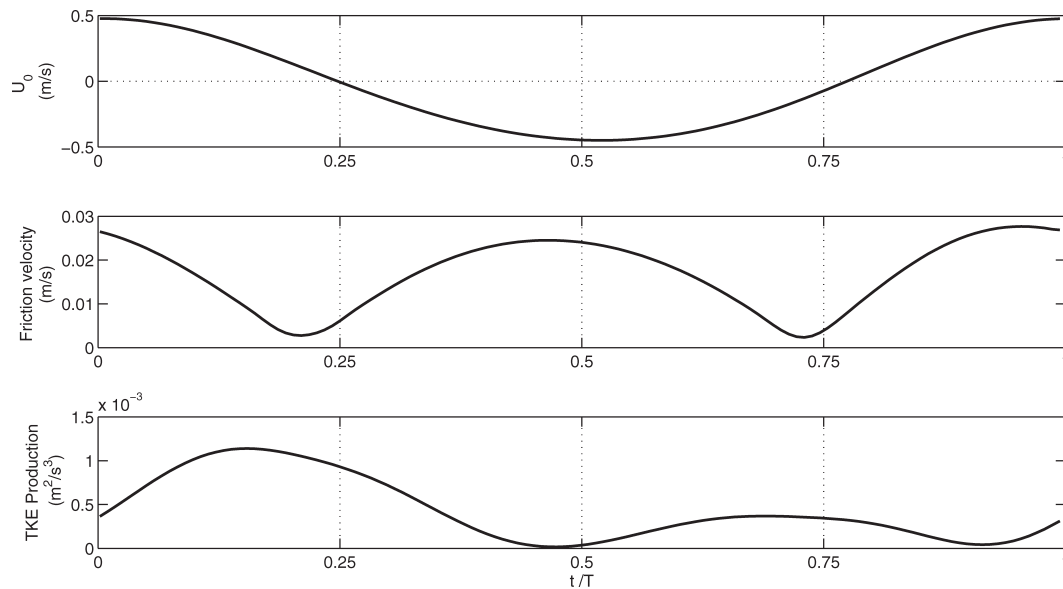


Figure 13. (top) Intrawave variations of free stream velocity, (middle) friction velocity, and (bottom) near-bed TKE production (case C1 presented here).

production to illustrate potential advantages and drawbacks of different approaches for sediment pickup. In particular, the friction velocity and thus the bed shear stress reach maximum values near maximum velocity, not near flow reversals. In comparison, the near-bed TKE production reaches maximum values shortly before flow reversals, which could result in better intrawave near-bed concentration predictions.

5. Conclusions

[54] We have presented a two-dimensional model that can be used as a numerical wave flume and provides predictions for wave propagation, flow velocities, turbulence, and sediment concentration. This model was implemented to reproduce experiments that were conducted in a large-scale wave flume [Williams *et al.*, 2000]. Model-data comparisons have shown that the model possesses reasonably good default predictive capability above dynamically flat beds. This is much less the case above steep ripples, where near-bed comparisons exhibit significant discrepancies.

[55] We have employed the model as a numerical diagnostic tool in order to directly assess parameterizations of key suspension processes above rippled beds and to investigate the inherent sensitivity to sediment transport formulations. Numerical results have shown that a simple increase in the roughness is not sufficient to obtain good predictions above steep ripples. Some other parameterization of the vortex entrainment process is necessary. Doing so by modifying directly the sediment diffusivity has resulted in improved results for wave-averaged suspended concentrations, but still fails to capture the impact of the steep ripples on the wave-averaged turbulent kinetic energy. The vortex entrainment process above steep ripples was observed to significantly modify the spectral characteristics of the near bed turbulence. The combination of model-data comparisons for flow velocity, sediment concentration, and turbulent kinetic energy thus indicates that a parameterization of vortex entrainment ought to primarily increase turbulent ki-

netic energy near the bed, and then change sediment diffusivity and suspended concentration in turn. This is consistent with existing detailed studies of the vortical processes above ripples.

[56] The parameterizations employed in the present study have led to significant improvement in the predictive ability for wave-averaged suspension above rippled beds. These results are pertinent not only for phase-resolving coastal models, but are also critical for the numerous coastal models that resolve neither intrripple lengthscales nor intrawave processes. Finally, progress in terms of the intrawave behavior of suspension still requires advances for the intrawave parameterizations of sediment pickup and sediment mixing.

[57] **Acknowledgments.** The authors acknowledge Jon J. Williams, who coordinated the experiments conducted in the Deltaflume under Hydralab funding, and Philip L.-F. Liu, who provided access to the COBRAS source code. The present work has been supported via core funding from the Natural Environment Research Council (NERC) to the National Oceanography Centre, and a NERC New Investigator grant (NE/J004499/1) awarded to L. O. Amoudry.

References

- Amoudry, L. O., and P. L.-F. Liu (2010), Parameterization of near-bed processes under collinear wave and current flows from a two-phase sheet flow model, *Cont. Shelf Res.*, *30*, 1403–1416.
- Amoudry, L. O., and A. J. Souza (2011), Deterministic coastal morphological and sediment transport modeling. A review and discussion, *Rev. Geophys.*, *49*, RG2002, doi:10.1019/2010RG000341.
- Amoudry, L., T.-J. Hsu, and P. L.-F. Liu (2005), Schmidt number and near-bed boundary condition effects on a two-phase dilute sediment transport model, *J. Geophys. Res.*, *110*, C09003, doi:10.1029/2004JC002798.
- Barr, B. C., D. N. Slinn, T. Pierro, and K. B. Winters (2004), Numerical simulation of turbulent, oscillatory flow over sand ripples, *J. Geophys. Res.*, *109*, C09009, doi:10.1029/2002JC001709.
- Blondeaux, P., P. Scandura, and G. Vittori (2004), Coherent structures in an oscillatory separated flow: numerical experiments, *J. Fluid Mech.*, *518*, 215–229.
- Chang, Y. S., and A. Scotti (2004), Modeling unsteady turbulent flows over ripples: Reynolds-averaged Navier-Stokes equations (RANS) versus

- large-eddy simulation (LES), *J. Geophys. Res.*, *109*, C09012, doi:10.1029/2003JC002208.
- Chorin, A. J. (1968), Numerical solution of the Navier-Stokes equations, *Math. Comput.*, *22*(104), 745–762.
- Davies, A. G., and P. D. Thorne (2005), Modeling and measurement of sediment transport by waves in the vortex ripple regime, *J. Geophys. Res.*, *110*, C05017, doi:10.1029/2004JC002468.
- Davies, A. G., and C. Villaret (1999), Eulerian drift induced by progressive waves above rippled and very rough beds, *J. Geophys. Res.*, *104*(C1), 1465–1488.
- Dimas, A. A., and G. A. Kolokythas (2011), Flow dynamics and bed resistance of wave propagation over bed ripples, *J. Waterw., Port Coastal Ocean Eng.*, *137*(2), 64–74.
- Fredsøe, J., K. H. Andersen, and B. M. Sommer (1999), Wave plus current over a ripple-covered bed, *Coastal Eng.*, *38*, 177–221.
- Garcia, M., and G. Parker (1991), Entrainment of bed sediment into suspension, *J. Hydraul. Eng.*, *117*(4), 414–435.
- Hagatun, K., and K. J. Eidsvik (1986), Oscillating turbulent boundary layer with suspended sediments, *J. Geophys. Res.*, *91*(C11), 13,045–13,055.
- Hansen, E. A., J. Fredsøe, and R. Deigaard (1994), Distribution of suspended sediment over wave-generated ripples, *J. Waterw. Port Coastal Ocean Eng.*, *120*(1), 37–55.
- Hirt, C. W., and B. D. Nichols (1981), Volume of fluid method for the dynamics of free boundaries, *J. Comput. Phys.*, *39*, 201–225.
- Huang, C.-J., C.-H. Chen, and H.-H. Chang (2011), Propagation of water waves over permeable rippled beds, *Ocean Eng.*, *38*, 579–591.
- Hurthel, D., and P. D. Thorne (2011), Suspension and near-bed load sediment transport processes above a migrating, sand-rippled bed under shoaling waves, *J. Geophys. Res.*, *116*, C07001, doi:10.1029/2010JC006774.
- Lin, P., and P. L.-F. Liu (1998a), A numerical study of breaking waves in the surf zone, *J. Fluid Mech.*, *359*, 239–264.
- Lin, P., and P. L.-F. Liu (1998b), Turbulence transport, vorticity dynamics, and solute mixing under plunging breaking waves in surf zone, *J. Geophys. Res.*, *103*(C8), 15,677–15,694.
- Lin, P., and P. L.-F. Liu (1999), Internal wave-maker for Navier-Stokes equations models, *J. Waterw. Port Coastal Ocean Eng.*, *125*(4), 207–215.
- Longuet-Higgins, M. (1981), Oscillating flow over steep sand ripples, *J. Fluid Mech.*, *107*, 1–35.
- Malarkey, J., and A. G. Davies (2002), Discrete vortex modelling of oscillatory flow over ripples, *Appl. Ocean Res.*, *24*, 127–145.
- Malarkey, J., and A. G. Davies (2004), An eddy viscosity formulation for oscillatory flow over vortex ripples, *J. Geophys. Res.*, *109*, C12016, doi:10.1029/2003JC002086.
- Mellor, G. (2002), Oscillatory bottom boundary layers, *J. Phys. Oceanogr.*, *32*(11), 3075–3088.
- Nielsen, P. (1992), *Coastal Bottom Boundary Layers and Sediment Transport*, World Scientific, Singapore.
- O'Hara Murray, R. B., P. D. Thorne, and D. M. Hodgson (2011), Intrawave observations of sediment entrainment processes above sand ripples under irregular waves, *J. Geophys. Res.*, *116*, C01001, doi:10.1029/2010JC006216.
- Osborne, P. D., and C. E. Vincent (1996), Vertical and horizontal structure in suspended sand concentrations and wave-induced fluxes over bedforms, *Mar. Geol.*, *131*, 195–208.
- Savioli, J., and P. Justesen (1997), Sediment in oscillatory flows over a plane bed, *J. Hydraul. Res.*, *35*(2), 177–190.
- Scandura, P., G. Vittori, and P. Blondeaux (2000), Three-dimensional oscillatory flow over steep ripples, *J. Fluid Mech.*, *412*, 355–378.
- Shih, T.-H., J. Zhu, and J. L. Lumley (1996), Calculation of wall-bounded complex flows and free shear flows, *Int. J. Numer. Methods Fluids*, *23*, 1133–1144.
- Sleath, J. F. A. (1991), Velocities and shear stresses in wave-current flows, *J. Geophys. Res.*, *96*(C8), 15,237–15,244.
- Thorne, P. D., J. J. Williams, and A. G. Davies (2002), Suspended sediments under waves measured in a large-scale flume facility, *J. Geophys. Res.*, *107*(C8), doi:10.1029/2001JC000988.
- Thorne, P. D., A. G. Davies, and J. J. Williams (2003), Measurements of near-bed intra-wave sediment entrainment above vortex ripples, *Geophys. Res. Lett.*, *30*(20), 2028, doi:10.1029/2003GL018427.
- Thorne, P. D., A. G. Davies, and P. S. Bell (2009), Observations and analysis of sediment diffusivity profiles over sandy rippled beds under waves, *J. Geophys. Res.*, *114*, C02023, doi:10.1029/2008JC004944.
- Torres-Freyermuth, A., I. J. Losada, and J. L. Lara (2007), Modeling of surf zone processes on a natural beach using Reynolds-averaged Navier-Stokes equations, *J. Geophys. Res.*, *112*, C09014, doi:10.1029/2006JC004050.
- van Rijn, L. C. (1984), Sediment transport, part II: Suspended load transport, *J. Hydraul. Eng.*, *110*(11), 1613–1641.
- van Rijn, L. C. (2007), Unified view of sediment transport by currents and waves. II: Suspended transport, *J. Hydraul. Eng.*, *133*(6), 668–688.
- van der Werf, J. J., V. Magar, J. Malarkey, K. Guizien, and T. O'Donoghue (2008), 2DV modelling of sediment transport processes over full-scale ripples in regular asymmetric oscillatory flow, *Cont. Shelf Res.*, *28*, 1040–1056.
- Vittori, G. (2003), Sediment suspension due to waves, *J. Geophys. Res.*, *108*(C6), 3173, doi:10.1029/2002JD001378.
- Williams, J. J., P. S. Bell, P. D. Thorne, K. Trouw, P. J. Hardcastle, and J. D. Humphery (2000), Observed and predicted vertical suspended sediment concentration profiles and bedforms in oscillatory-only flow, *J. Coastal Res.*, *16*(3), 698–708.
- Williams, J. J., P. S. Bell, P. D. Thorne, N. Metje, and L. E. Coates (2004), Measurement and prediction of wave-generated suborbital ripples, *J. Geophys. Res.*, *109*, C02004, doi:10.1029/2003JC001882.
- Zedler, E. A., and R. L. Street (2006), Sediment transport over ripples in oscillatory flow, *J. Hydraul. Eng.*, *132*(2), 180–193.
- Zyserman, J. A., and J. Fredsøe (1994), Data analysis of bed concentration of suspended sediment, *J. Hydraul. Eng.*, *120*(9), 1021–1042.